NJC

PAPER

View Article Online
View Journal | View Issue

Cite this: *New J. Chem.*, 2015, 39, 8035

A highly efficient non-enzymatic glucose biosensor based on a nanostructured $NiTiO_3$/NiO material

Nabanita Pal,*[a] Barnamala Saha,[a] Sudipta K. Kundu,[b] Asim Bhaumik[b] and Sangam Banerjee[a]

Received (in Montpellier, France) 29th May 2015,
Accepted 30th July 2015

DOI: 10.1039/c5nj01341k

www.rsc.org/njc

An efficient and novel non-enzymatic glucose sensing platform composed of self-assembled crystalline $NiTiO_3$/NiO nanoparticles is reported in this article. The mixed oxide nanoparticles have been synthesized using a facile sol–gel method mediated by evaporation induced self-assembly (EISA) in non-aqueous media. After annealing at 673 K the final product obtained was well characterized using various analytical tools like powder X-ray diffraction (PXRD) and scanning and transmission electron microscopy (SEM and TEM), along with energy dispersive X-ray spectroscopy (EDS)and UV-visible diffuse reflectance spectroscopy (DRS) studies which reveal that the nanomaterial is composed of *ca.* 30–35 nm sized nanocrystals that have an ilmenite $NiTiO_3$ structural phase with some percentage of bunsenite NiO. The $NiTiO_3$/NiO nanoparticles exhibit an outstanding electro-catalytic activity towards glucose oxidation in 0.1 M NaOH alkaline media at an applied potential of +0.55 V (*vs.* Ag/AgCl electrode). The glucose sensing investigation of this Ni–Ti electrode indicates a very high sensitivity and a low limit of detection (LOD) of 1454 μA mM^{-1} cm^{-2} and 0.06 μM, respectively. The glucose level in human blood serum was also tested with our sample which produced a satisfactory result. Thus, the $NiTiO_3$/NiO electrode can be used as a highly effective, economical, stable and non-air sensitive platform for non-enzymatic glucose detection.

Introduction

Self-assembled nanostructured building blocks of different dimensions arranged together by weak natural forces like van der Waals forces,[1] H-bonding interactions,[2] electrostatics,[3] host–guest interactions[4] *etc.* are a growing area of research for budding scientists as they have great potential in some pioneering fields like catalysis, optics, microelectronics, magnetism, sensing and so forth.[5–7] In addition, as they possess a larger surface to volume ratio than their corresponding bulk material, these nanoparticles possess some unique properties like quantum effects, macroscopic quantum tunnelling effects *etc.*[8] and find important applications in electrochemical devices such as supercapacitors, batteries and in biological and chemical sensors.[9–11] Numerous chemical methods such as hydrothermal, evaporation induced self-assembly (EISA), microwave assisted heating and microemulsion techniques have been employed recently in the fabrication of different self-organized metal, metal oxide, mixed oxide, metal sulfide, selenide and chalcogenide nanoparticles.[12–15] Sometimes, a tri-block copolymer (Pluronic P123, F127) can be used as a stabilizing agent to control the growth of nanoparticles during the synthesis process and at the final stage the polymer can be removed from the solid composite material to yield small well-organized nanoparticles.[16,17] A number of self-assembled crystalline metal oxide and mixed oxide nanoparticles synthesized using a Pluronic template, *e.g.* ZrO_2,[18] TiO_2,[19] NiO–ZrO_2,[20] $SrTiO_3$,[21] CeO_2[22] *etc.* have been reported to date. Transition metal titanates, *e.g.* ilmenite $NiTiO_3$, are highly fascinating materials because of their contribution in a wide range of applied fields like photocatalysis,[23] solid oxide fuel cells,[24] catalysis,[25] gas sensing,[26] pigments,[27] dielectric materials[28] *etc.* The synthesis of ilmenite $NiTiO_3$ thin films, powders and nanorods using different methods is reported in the literature by various scientists.[23–30] But to the best of our knowledge, an EISA mediated synthesis of self-assembled highly stable ilmenite $NiTiO_3$/NiO nanocrystalline frameworks has rarely been reported.

The accurate monitoring of glucose levels in blood is necessary to control complicated diseases like diabetes, kidney problems, *etc.*[31] For this clinical purpose, various sensitive, selective, and inexpensive amperometric biosensors for glucose have been developed by immobilizing glucose oxidase (GOD) enzymes in different matrices.[32] However, though these conventional enzyme based glucose sensors show high sensitivity and selectivity, they usually suffer from some limitations such as instability and complex enzyme immobilization procedures, as well as their performance being highly sensitive to variations of temperature,

[a] *Surface Physics and Materials Science Division, Saha Institute of Nuclear Physics, Block-AF, Sector-I, Bidhannagar, Kolkata-700064, India. E-mail: nabanita.pal@saha.ac.in, pal_nabamsc@yahoo.co.in*
[b] *Department of Materials Science, Indian Association for the Cultivation of Science, Jadavpur, Kolkata-700 032, India*

humidity, pH and the composition of the substrate.[33] Hence, metal or metal oxide based non-enzymatic glucose sensing is highly desirable as well as a reliable, fast and convenient method for measuring glucose concentration in clinical biochemistry and the food industry.[12,34] Nanostructured metal oxides have high surface reactivity, excellent catalytic activity as well as exceptional optical and electrical properties on account of their electron and photon confinement, which makes these materials highly effective in the development of a biosensor.[35] Since Fleischmann's demonstration of glucose molecule oxidation at a nickel anode in alkaline solution,[36] nanostructured Ni, NiO and $Ni(OH)_2$-based electrodes are widely utilized for the electrochemical detection of glucose in a non-enzymatic way.[37–39] However, the sensitivity observed was not so high in those cases. In the case of Ti-based nanostructures, they do not show good electrochemical activity due to the poor conductivity of TiO_2.[40] As a consequence, there is always ongoing research for increasing the electrochemical performance of TiO_2 by inserting other conducting ions in it to form a highly sensitive biosensing material. For example, carbon-doped TiO_2 nanotube arrays exhibit outstanding electrochemical performance with high sensitivity and selectivity.[40] The doping of Ni and NiO in Ti-based materials to increase biosensing performance is also observed in the literature. Recently, Gao *et al.* reported a self-organized nanoporous NiO/TiO_2 layered material with high stability and a sensitivity of 252 $\mu A\ mM^{-1}\ cm^{-2}$ for non-enzymatic glucose sensing.[41] $Ni/NiTiO_3/TiO_2$ nanotube arrays reported by Huo *et al.* have also been proved to be highly efficient (sensitivity: 438.4 $\mu A\ mM^{-1}\ cm^{-2}$) as non-enzymatic glucose biosensor devices.[42] Though the sensitivity of the sensors and limits of detection were not so high in either case, the idea of these works has motivated us to construct a highly sensitive, stable non-enzymatic glucose monitoring platform based on a Ni and Ti nanostructured material.

Herein, our study describes a simple EISA method for the preparation of a highly crystalline ilmenite $NiTiO_3$ nanostructure with a rhombohedral structure which exhibits very high sensitivity and a low limit of detection for non-enzymatic glucose sensing. Common interfering species such as ascorbic acid (AA), dopamine (DA) and uric acid (UA) do not have any significant influence in this analysis and a practical test performed with human blood serum provides a well-matched result of blood glucose levels with that of a commercial glucometer.

Experimental section

Materials

Pluronic F127 (M_{av} = 12 600, $EO_{106}PO_{70}EO_{106}$, Sigma-Aldrich) was used as a stabilizer, 35 wt% hydrochloric acid (HCl, E-Merck) was used to maintain the acidity of the medium and citric acid (E-Merck, India) was used as a capping agent. Nickel(II) nitrate hexahydrate, $(Ni(NO_3)_2{\cdot}6H_2O)$ (Loba Chemie, India) and titanium(IV) butoxide $[Ti(OC_4H_9)_4$, Sigma-Aldrich] were used as the nickel and titanium precursors, respectively. 5 wt% Nafion solution (Sigma-Aldrich), dextrose (SRL, India), ascorbic acid (AA, Merck, India), uric acid (UA, Loba Chemie, India) and dopamine (DA, Sigma-Aldrich) were employed for various electrochemical analyses. All the chemicals were used as received without further purification.

Synthesis of Ni–Ti nanostructures

In a typical synthesis of the Ni–Ti sample (Ni : Ti molar ratio = 1 : 1), 1 g of Pluronic F127 was dissolved in 20 mL of ethanol solvent by using 1.65 g of HCl solution followed by the addition of 0.63 g of citric acid. This solution was stirred vigorously for 1.5 to 2 h at room temperature (RT) before the addition of 2.95 g (10 mmol) of $Ni(NO_3)_2$ salt. The mixture was stirred until all of the Ni salt dissolved yielding a clear green solution. Next, 3.41 g (10 mmol) of $Ti(OC_4H_9)_4$ solution was added to the mixture dropwise with continuous stirring. The resulting mixture was kept stirring and covered with aluminium foil overnight and was aged successively at RT and elevated temperature (333 K) under quiescent conditions. Evaporation of the solvent during this ageing process yielded a solid green product. The material was annealed at 673 K for 5 h in the presence of air to remove the Pluronic co-polymer and enhance the adhesion between particles. Finally, the material obtained as a deep green powder was named NT773. A sample was also heated at 1073 K which was named NT1073. Another Ni–Ti sample (Ni : Ti molar ratio = 1 : 2) was prepared following a similar procedure using 5 mmol of Ni precursor instead of 10 mmol. The sample annealed at 773 K was named NT12.

Characterization of Ni–Ti samples

The wide angle powder X-ray diffraction (XRD) patterns of the NT773, NT1073 and NT12 nanocomposite materials were recorded on a Bruker AXS D-8 Advance diffractometer operated at a 40 kV voltage and 40 mA current and calibrated with a standard silicon sample, using Ni-filtered Cu Kα (λ = 0.15406 nm) radiation. The sample was prepared by grinding and then placed on the sample holder at room temperature. The spectra were recorded against 2θ from 15 to 70 degrees with a scan step of 0.10.

A JEOL JEM 6700F field emission scanning electron microscope (FE SEM) with an energy dispersive X-ray spectroscopic (EDS) attachment was used to analyze the morphology of the sample and its surface chemical composition. A layer of powder sample was brushed homogeneously on the carbon tape for performing the analysis.

UHR-TEM images of the NT773 sample were recorded on a JEOL 2010F TEM operated at 200 kV. Prior to the measurement a small pinch of the sample was ultrasonicated in ethanol for 10 min and dropped on a Cu-grid which was dried in air.

Nitrogen adsorption–desorption isotherms of the NT773 sample were recorded at 77 K using a Quantachrome Autosorb 1C instrument. The sample was degassed at 373 K under vacuum before the measurement. The BET (Brunauer–Emmett–Teller) specific surface area was evaluated from the sorption data in a relative pressure (P/P_0) range from 0.05 to 0.16. A pore size distribution (PSD) curve was obtained from the isotherms by using a non-local density functional theory (NLDFT) method.

UV-visible diffuse reflectance spectra were recorded using a Shimadzu UV 2401PC spectrophotometer with an integrated

sphere attachment. The sample analyzed was in a dry state and the measurement was carried out at room temperature using a $BaSO_4$ pellet as the background standard.

Ni and Ti content in the NT773 sample was measured on a Shimadzu AA-6300 atomic absorption spectrophotometer (AAS) using air/C_2H_2 and N_2O/C_2H_2 flames, respectively. Prior to the analysis an aqueous solution of the sample was prepared by digesting 10 mg of powder sample in the minimum quantity of HF/HNO_3 and then diluting it with 100 mL water.

Preparation of the glucose biosensor and its electrochemical behavior

A three-electrode electrochemical cell consisting of Ag/AgCl as the reference electrode (1 M KCl), NT773-modified ITO glass (area = 6 × 7 mm^2) as the working electrode, and Pt wire as the counter electrode was used as the glucose biosensing device in the laboratory. Before sampling, to prepare NT773-modified-ITO, first the ITO (indium-tin oxide) coated glass slide was cleaned with ultrasonication in ethanol and deionized water for 10 min, respectively and dried in air. A homogeneous slurry of the NT773 powder was prepared by ultrasonicating about 20 mg of the sample in a few drops of ethanol. Then the slurry was added dropwise on the working ITO electrode, left to dry at room temperature, after which one or two drops of 0.5% Nafion binder solution was placed on the sample layer to fix the material on the ITO electrode. Finally the electrode was dried overnight in air to obtain NT773 modified-ITO for the electrochemical measurements.

All of the electrochemical experiments were performed at room temperature on a CHI660c electrochemical workstation (CH Instruments Inc., USA). Cyclic voltammetric (CV) analyses were carried out at a scanning rate of 50 mV s^{-1} between +0.2 and +0.7 V using 0.1 M NaOH solution as a background electrolyte. For each CV test, 0.1 mL of freshly prepared aqueous glucose solution was added in 10 mL of 0.1 M NaOH medium. Amperometric *i–t* responses at an applied potential of +0.55 V were recorded in a similar fashion by stirring the solution homogeneously. The electrodes were washed with fresh water and air dried between every analysis to prevent contamination from the prior measurement.

Ethical statement

All experiments involving the use of human subjects were performed in compliance with the relevant laws and institutional guidelines. Consent was obtained from the human subject and the Saha Institute of Nuclear Physics approved the experiments.

Results and discussion

Two samples of Ni–Ti powder nanocrystals were prepared *via* an evaporation induced self-assembly (EISA) method using a non-ionic Pluronic F127 surfactant, nickel(II) nitrate and titanium(IV) butoxide precursors in non-aqueous ethanolic media in the presence of a citric acid complexing agent. The molar ratios of Ni and Ti in the synthesis gel were 1 : 1 and 1 : 2, respectively. The characterizations were performed using the samples after annealing at 773 K under flowing air. A thorough glucose sensing investigation were carried out on the NT773 sample using different electrochemical measurements in 0.1 M NaOH solution by preparing a three-electrode cell consisting of NT773-modified ITO as the working electrode, Ag/AgCl as the reference electrode and Pt wire as the counter electrode.

Crystallinity and structural phase analysis

Wide angle X-ray diffraction (WAXRD) patterns were recorded to determine the crystalline structure and phase of the Ni–Ti samples synthesized using the EISA method are displayed in Fig. 1. Strong diffraction peaks for the NT773 and NT1073 samples after thermal treatment at temperatures of 773 K and 1073 K are observed in the respective XRD data shown in Fig. 1(a) and (b). Annealing at 773 K yields a highly crystalline oxide nanocomposite structure, revealing intense peaks (Fig. 1(a)). The diffraction peaks correspond to a predominating crystalline phase of a rhombohedral (trigonal) structure of ilmenite $NiTiO_3$.[23] The strongest characteristic peaks are matched well with JCPDS file no. 033-0960 (trigonal, $a = b$ = 5.03 Å, c = 13.79 Å, V = 302.19 $Å^3$) representing the typical reflection planes (012), (104), (110), (113), (024), (116), (018), (214) and (300) situated at 2θ = 24.1°, 33.0°, 35.6°, 40.9°, 49.4°, 54.0°, 57.4°, 62.5° and 64.2°, respectively. In addition, a small amount of NiO was present in the material as represented by the sharp peaks at 2θ = 37.2° and 43.3° corresponding to the crystal planes (111) and (200) of a bunsenite NiO (JCPDS No. 04-0835) phase. When the material was heated further at a higher temperature (1073 K), the XRD pattern does not show any significant change except for a small increase in the relative intensities of the $NiTiO_3$/NiO peaks. Additionally, a small impurity peak of anatase TiO_2 (JCPDS No. 21-1272) was also present in the NT773 sample which had been changed to rutile

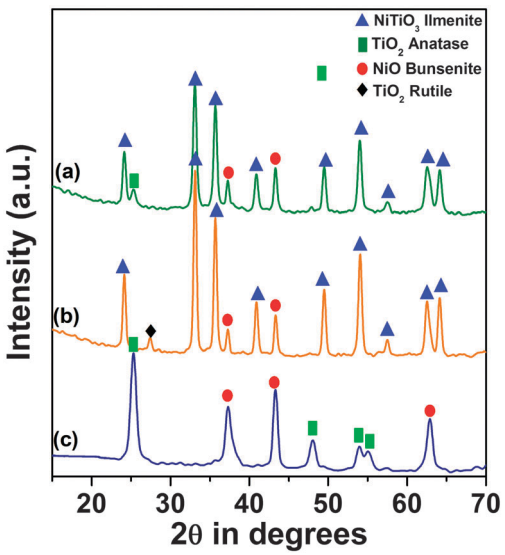

Fig. 1 Wide angle powder X-ray diffraction (WAXRD) pattern of the $NiTiO_3$/NiO nanoparticles (a) at 773 K and (b) at 1073 K. (c) WAXRD pattern of the NT12 sample after annealing at 773 K. The peaks are indexed according to the corresponding JCPDS data.

TiO_2 (JCPDS No. 21-1276) upon high temperature treatment. Hence, it is clearly evident from the WAXRD analysis that a composite phase of $NiTiO_3$/NiO with a predominating percentage of $NiTiO_3$ nanoparticles is formed during the sol–gel synthesis, with a Ni : Ti = 1 : 1 molar ratio *via* the EISA method followed by heating (at 773 K) in air, and that the material composite is highly stable up to 1073 K. On the other hand, Fig. 1(c) shows the WAXRD pattern of the NT12 sample with a Ni : Ti molar ratio = 1 : 2 after heating at 773 K. No diffraction peaks for the ilmenite $NiTiO_3$ phase are present here, instead a mixed crystalline phase of anatase TiO_2 (JCPDS No. 21-1272) and bunsenite NiO (JCPDS No. 04-0835) nanostructures is observed without the domination of any single phase. Hence, considering the contribution of the $NiTiO_3$ phase in the literature, we discarded the NT12 sample and performed the other characterization techniques as well as the sensing study with the NT773 sample prepared using a Ni : Ti = 1 : 1 ratio.

Morphology and elemental composition

A FESEM study of the sample was performed to investigate the morphology of the $NiTiO_3$/NiO material. The representative SEM image of the sample shown in Fig. 2A indicates that small spherical particles are homogeneously distributed throughout the specimen and in some places they aggregated to form large clusters.

The EDS image of the NT773 sample showing the presence of Ni, Ti and O is presented in Fig. 2B. From the EDS results the atomic percentage ratio of Ni : Ti in the calcined product obtained is 1 : 1.14 which resembles well with the molar percentage ratio of Ni and Ti (1 : 1) used for the synthesis gel (Table 1).

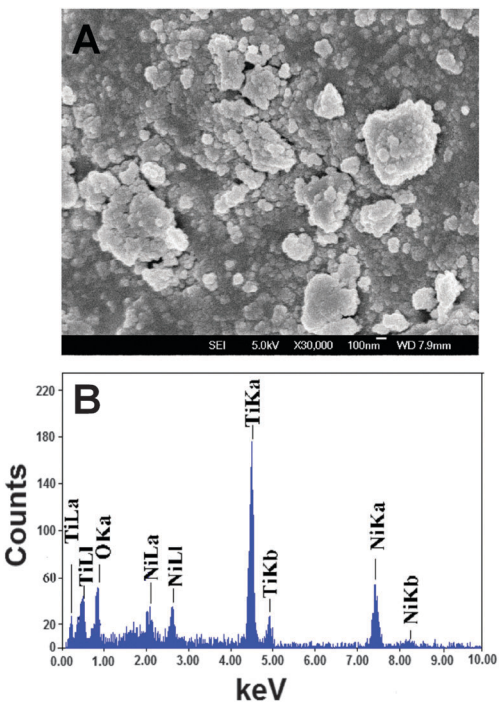

Fig. 2 (A) FESEM image of the NT773 nanoparticles. (B) EDS image of the nanocomposite sample showing the presence of Ni, Ti and O species.

Table 1 Physicochemical data of the $NiTiO_3$/NiO nanocomposite sample (NT773)[a]

$f_{Ni:Ti}$	$F_{Ni:Ti}$	$A_{Ni:Ti}$	S_{BET} ($m^2\ g^{-1}$)	V_p ($cm^3\ g^{-1}$)	D_p (nm)	r (nm)
1 : 1	1 : 1.14	1 : 0.7	66	0.092	3.60	30–35

[a] Notation: $f_{Ni:Ti}$ = molar ratio of the Ni to Ti precursors used in the synthesis gel; $F_{Ni:Ti}$ = molar ratio of the Ni to Ti species in the final product (measured by EDS), $A_{Ni:Ti}$ = Ni and Ti atomic percentage ratio obtained from the AAS measurements, S_{BET} = BET specific surface area determined in the relative pressure range of 0.06 to 0.26; V_p = single-point pore volume measured from the sorption data; D_p = pore diameter at the maximum of the PSD curve obtained using the NLDFT method; r = average diameter of the particles observed in the TEM image.

Nanostructure study

In order to get a good indication of the structural features of ilmenite $NiTiO_3$ nanoparticles at the atomic level, TEM and high resolution TEM analyses were performed on our sample. In Fig. 3(A–C) the TEM images of the sample NT773 at different resolutions are shown. The images indicate regular spherical type particles distributed throughout the specimen. A closer look at the image shows the crystal fringes of the particles in Fig. 3C. Selected area electron diffraction (SAED) pattern of the sample obtained from the HRTEM images is depicted in Fig. 3D which clearly demonstrates a number of diffraction spots representing several planes, the diameter of the planes corresponds to the *d*-spacing values of the ilmenite $NiTiO_3$ and bunsenite NiO phases as obtained from the PXRD patterns. So, the TEM analysis data indicate that self-aggregated $NiTiO_3$ mixed oxide nanoparticles along with the NiO phase have been formed during the EISA method.

Surface area and pore size analysis

The representative N_2 adsorption–desorption isotherms used to evaluate the BET specific surface area, pore volume, and average

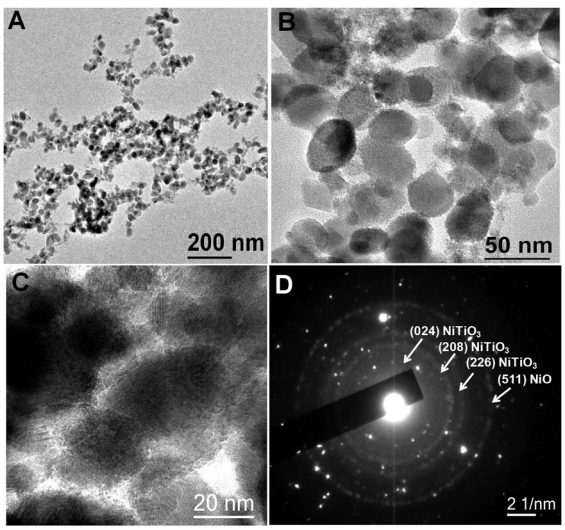

Fig. 3 (A–C) TEM image of the ilmenite $NiTiO_3$/NiO composite nanoparticles (NT773) synthesized using the EISA method in various magnifications. (D) SAED (selected area electron diffraction) pattern of the NT773 sample.

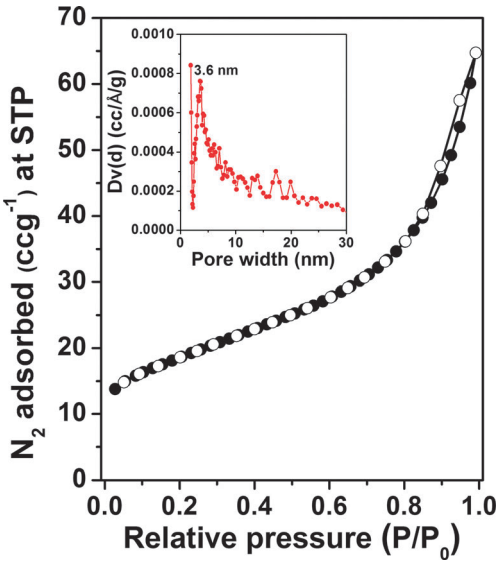

Fig. 4 Nitrogen adsorption (●)/desorption (○) isotherms of the NT773 sample measured at 77 K. The pore size distribution (PSD) curve of the sample (measured by the NLDFT method), representing the pore diameter is shown in the inset.

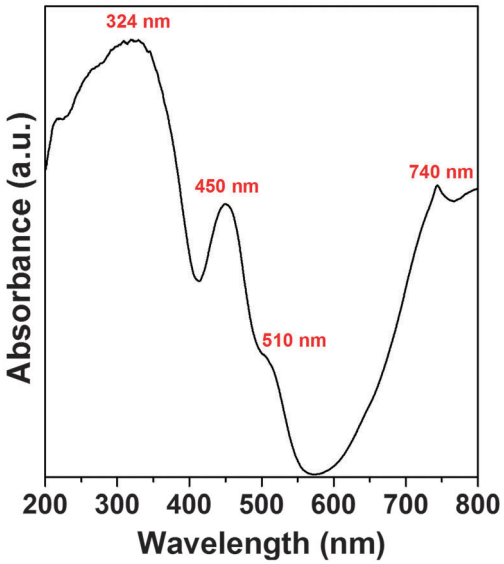

Fig. 5 UV-visible diffuse reflectance spectrum (DRS) of the $NiTiO_3$/NiO sample recorded at room temperature.

pore diameter of the self-assembled $NiTiO_3$/NiO nanocomposite material are shown in Fig. 4. Table 1 shows the related physico-chemical parameters estimated from this sorption analysis. The isotherm loops of NT773 show a typical type II pattern, according to the conventional IUPAC classification. The BET surface area (S_{BET}) and the total pore volume (V_p) obtained for the material are 66 $m^2\ g^{-1}$ and 0.092 $cm^3\ g^{-1}$, respectively.

A pore size distribution plot evaluated by applying the NLDFT (non-local density functional theory) method is shown in the inset of Fig. 4. A PSD pattern representing an average pore diameter (D_p) value of 3.60 nm is observed in this case (Table 1) which implies that interparticle porosity may be present in the material. But the interparticle porosity is not uniform throughout the whole sample which is clearly evident from the zigzag peak pattern of the PSD curve.

Percentage composition of the sample

Using the AAS technique we can find out the atomic percentage of the elements present in our material. The amount of Ni and Ti present in the NT773 sample was 11.76% and 8.09%, respectively. From this, the percentage ratio of $NiTiO_3$ to NiO in the evaluated NT773 sample is 11 : 1. The result is in good agreement with the WAXRD data and confirms that the $NiTiO_3$ phase predominates the composite phase of the $NiTiO_3$/NiO nanoparticles formed using the EISA method.

Chemical environment and electronic states of Ni and Ti species

Diffuse reflectance UV-visible spectra (DRS) provide valuable information about the coordination environment and oxidation states of the transition metal ions of mixed oxides. The representative DRS spectrum of the $NiTiO_3$/NiO composite nanoparticles measured in the range of 200–800 nm is displayed in Fig. 5. Three types of electronic transitions are expected in the $NiTiO_3$/NiO sample, represented as O 2p → Ti 3d, Ni 3d → Ti 3d and Ni 3d → O 2p bands.[43] Broad absorption peaks near ~324 nm, 450 and 740 nm with a small hump in the visible range ~510 nm are observed in this spectrum. The broad peak in the UV region can be attributed to the charge transfer transition from the O^{2-} 2p valence band to the Ti^{4+} 3d conduction band.[30,43] In addition, the other bands near the 450 and 510 nm regions are typically characteristic of the crystal field splitting of $NiTiO_3$ nanoparticles indicating $Ni^{2+} \rightarrow Ti^{4+}$ charge transfer (CT) bands obtained from the splitting of the $3d^8$ band of the Ni^{2+} ions.[43] The broad peak near the 740 nm region arises also due to the highly intense color of the $NiTiO_3$ species.[43]

Glucose sensing study

To study the non-enzymatic glucose sensing capability of our $NiTiO_3$/NiO composite material *via* electrocatalytic redox phenomena, electrochemical characterizations, *e.g.* CV and amperometry, were performed using the sample as the working electrode in a three-electrode cell system. The electrochemical behavior of the NT773-layered ITO electrode with and without addition of glucose analyte has been investigated using cyclic voltammetry (CV) in 0.1 M NaOH solution which is shown in Fig. 6A. The sample exhibits a good CV response in the potential region from 0.2 to 0.7 V compared to bare ITO, which is evident from the increased current (A) at a scanning rate of 50 mV s^{-1}. The voltammogram exhibits a well defined anodic peak at 0.54 V (*vs.* Ag/AgCl) representing the oxidation of $Ni^{II}(OH)_2$ to nickel oxy-hydroxide $Ni^{III}OOH$ in alkaline media and a cathodic peak at 0.38 V which is associated with the reversible conversion of Ni(III)oxy-hydroxide back to Ni(II)hydroxide. When 10 mM glucose was added, both the anodic and cathodic currents change abruptly along with a shift in the respective peak current. In contrast, no significant electrochemical response or any reversible

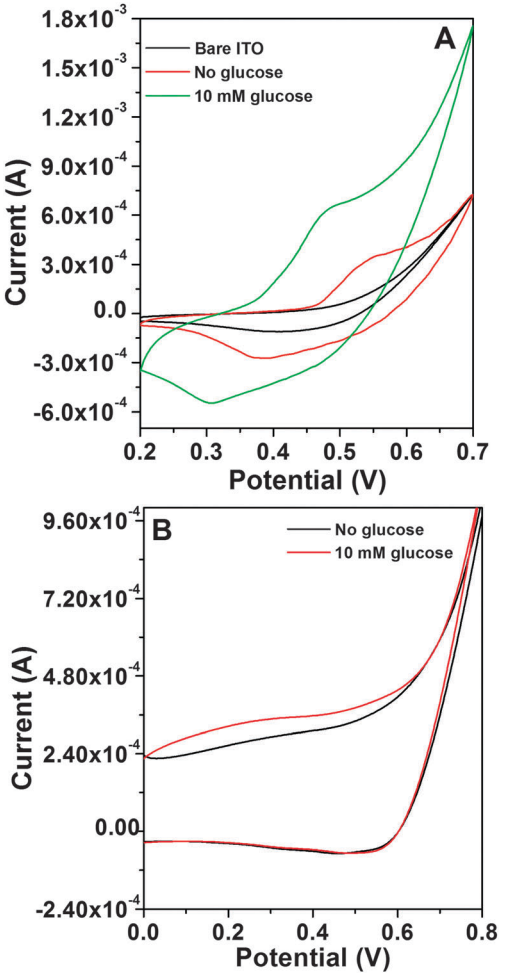

Fig. 6 Cyclic voltammetric response of (A) the $NiTiO_3$/NiO (NT773) sample and (B) the pure TiO_2 powder in 0.1 M NaOH electrolyte at a scan rate of 50 mV s^{-1}. The CV plot of bare ITO is also shown in (A).

redox reaction is observed in the case of the pure TiO_2-modified ITO electrode in the absence or in the presence of glucose as shown from the CV patterns in Fig. 6B. The electrochemical redox phenomena of Ni^{2+}/Ni^{3+} which occur at the working electrode surface in basic media and also in the presence of glucose analyte are suggested as follows:

$$NiO + OH^- \rightarrow NiO(OH) + e^- \quad (1)$$

$$NiO(OH) + \text{glucose} \rightarrow Ni(OH) + \text{glucolactone} \quad (2)$$

Thus, the electrooxidation of glucose to glucolactone by $Ni^{III}O(OH)$ formed in the alkaline media is responsible for the enhancement of the anodic peak current.[43]

CV curves of the NT773-ITO electrode were recorded with the addition of increasing glucose concentration in a 0.1 M supporting electrolyte (NaOH) at a scanning rate of 50 mV s^{-1} which are shown in Fig. 7. With successive injection of glucose, an increase in the anodic as well as in the cathodic current is observed herein demonstrating the oxidation and reduction of added glucose molecules. A gradual shift of the peak potential of the CV curves (positive shift in the oxidation peak and

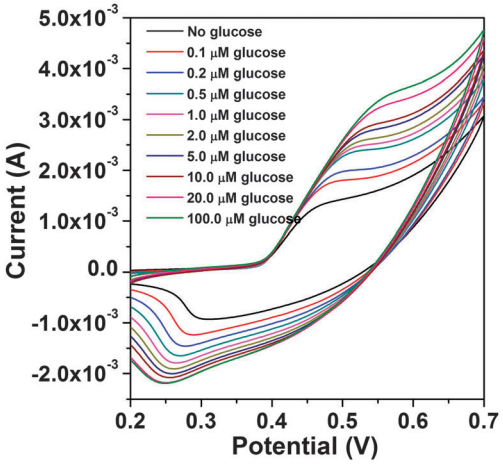

Fig. 7 Cyclic voltammograms (CV) of the $NiTiO_3$/NiO (NT773) material at a scan rate of 50 mV s^{-1} in 0.1 M NaOH solution and the response with successive addition of glucose solution.

negative shift in the reduction peak) is detected which enhances upon increasing the concentration of added glucose solutions clearly indicating the significant interaction of glucose with the electrode surface already covered with low valence nickel species.[46]

Fig. 8A presents a typical current–time (*i–t*) plot of the NT773-ITO electrode obtained from the amperometric response of the NiO–TiO_2 layered working electrode at room temperature (298 K) upon successive injection of glucose (concentration ranging from 0.1 μM to 0.1 mM) in a stirred 0.1 M NaOH solution at an applied potential 0.55 V (*vs.* Ag/AgCl). A well-defined stepwise increase in the oxidation current of the amperometric *i–t* curve even at very low concentrations of glucose implies a good electrocatalytic sensitivity of the porous nanoparticles. The corresponding current *vs.* concentration calibration curve is shown in the inset of Fig. 8A, which reveals the linear response. A wide range of complete *i–t* curve using glucose concentrations ranging from 0.1 μM to 2 mM has been displayed in Fig. 8B. In Fig. 8C the corresponding calibration curve is shown, from which it's clearly evident that the sample NT773 possesses two linear ranges for glucose oxidation: one from 0.1 to 25.0 μm with a correlation coefficient and sensitivity of 0.8754 and 1454 μA mM^{-1} cm^{-2}, respectively, and another for the concentration of 0.025 to 2.07 mM with a correlation coefficient of 0.9995 and a sensitivity 52.86 μA mM^{-1} cm^{-2}. The limit of detection (LOD) was evaluated as 0.06 μM. The current deviates from linearity at higher glucose concentration which may be due to the passivation of the electrode in alkaline media. A comparison of our sample with some other Ni-based glucose sensing electrodes reported in the literature is shown in Table 2.

For practical analysis, the $NiTiO_3$/NiO electrode (NT773-ITO) was applied in the evaluation of glucose concentration in human blood serum. The concentration of glucose in human blood serum collected from a volunteer was measured using an Accu-check active glucometer. Then the serum solution was diluted hundredfold to prepare a sample solution for our laboratory test. 0.2 mL of this diluted serum solution was

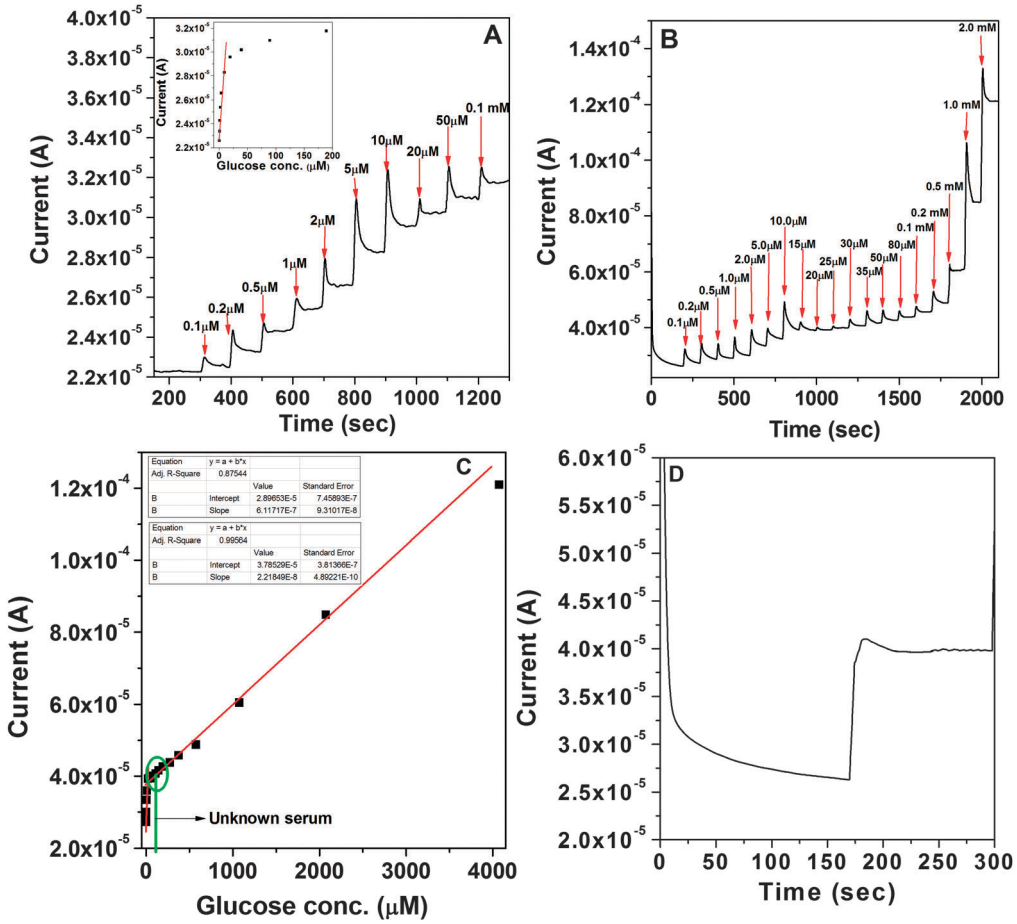

Fig. 8 (A) Amperometric response of the $NiTiO_3$/NiO working electrode in 0.1 M NaOH with a gradual injection of micromolar concentrations of glucose at an applied potential of +0.55 V. Respective calibration curve of the current *vs.* glucose concentration (in μM) is shown in the inset. (B) Amperometric response of the working electrode after successive injection of glucose (μM to mM) at a +0.55 V applied potential in 0.1 M NaOH solution. (C) Calibration curve and linear plot of current *versus* glucose concentration (μM). (D) Amperometric response of the current (A)–time (s) after addition of an unknown human blood serum solution at a +0.55 V potential in 0.1 M NaOH solution.

Table 2 Comparison of the sensing properties of the $NiTiO_3$/NiO composite sample with other Ni-based non-enzymatic glucose sensors reported in the literature

Electrode/sensor	Sensitivity[a] ($\mu A\ mM^{-1}\ cm^{-2}$)	LOD[b] (μM)	Background electrolyte	Linear range (mM)	Ref.
Nanoporous NiO/TiO_2 layers	252.0	1.0	0.1 M NaOH	0.005–12.1	41
Ti/TiO_2 nanotube array/Ni	200	4	0.1 M NaOH	0.1–1.7	37
NiO/C-Ti	582.6	2	0.1 M NaOH	0.002–2.6	39
Mesoporous Ni incorporated SBA-15	44.8	50	0.1 M NaOH	0.05–20	38
Ni/$NiTiO_3$/TiO_2 NTAs	438.4 & 323.6	0.7	1.0 M NaOH	0.005–0.5	42
Ni loaded carbon nanofiber paste	420.4	1	0.1 M NaOH	0.002–2.5	45
Nano-Ni$(OH)_2$ on graphite	2401	0.53	0.1 M NaOH	0.001–15	44
Self-assembled nano-$NiTiO_3$/NiO	1454 & 52.86	0.06	0.1 M NaOH	0.0001–0.0188 and 0.04–2.07	Present work

[a] Sensitivity = Slope of the calibration curve/used area of the working electrode. [b] LOD (Limit of detection) = [3 × standard deviation (SD) of the blank response/slope of the calibration curve]. Here, SD = 0.1178×10^{-7} and slope = 6.12×10^{-7}.

injected in 0.1 M NaOH solution and the current response was measured at 0.55 V (Fig. 8D). The corresponding concentration value of glucose obtained by extrapolating the current value in the calibration curve (green point in Fig. 8C) matches well with the result obtained from a commercial glucometer. Table 3 represents a comparison of the data from the glucometer and electrochemical detection. Thus the self-assembled $NiTiO_3$/NiO nanoparticle material can be used as a true glucose biosensing device.

In the case of non-enzymatic glucose sensing, during any practical experiments, the selectivity of the working electrode needs to be verified. Small amounts of other species like ascorbic acid (AA), uric acid (UA) and dopamine (DA) co-exist with glucose in human blood serum and may cause interference

Table 3 Amperometric detection of glucose in a human serum sample with our NT773 sensor

Glucose concentration in original serum measured using glucometer	Glucose concentration estimated in serum after dilution	Glucose concentration in diluted serum obtained from calibration curve	Difference in two results
179 mg dL^{-1} (9.9 mM)	0.099 mM	102 μM (0.102 mM)	0.003 mM

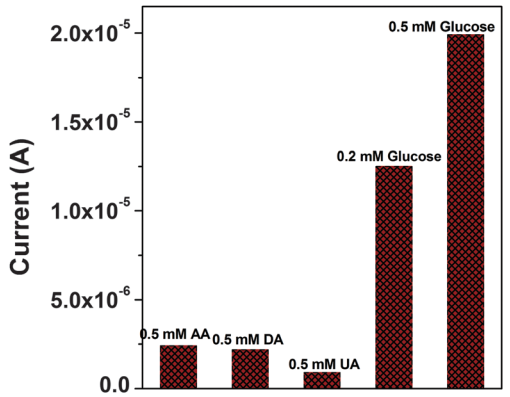

Fig. 9 Effect of interfering species like AA, DA and UA on the current response of the NT500 sample in 0.1 M NaOH at an applied potential of +0.55 V (*vs.* Ag/AgCl).

during glucose detection with non-enzymatic methods.[47] Fig. 9 shows a good selective determination of glucose with the NT773-ITO electrode upon addition of 0.5 mM of each interfering agent and 0.2 mM or 0.5 mM of glucose solution successively into a constantly stirred solution of 0.1 M NaOH during amperometry analysis. The response current for the interfering agents remains in the range 7.0–12.0% of that obtained from glucose. This result demonstrates that the presence of AA, UA or DA has no significant influence or interference on the oxidation current response for 0.2 mM or 0.5 mM glucose in 0.1 M NaOH media. Thus, $NiTiO_3$/NiO composite nanoparticles have been proved to be a satisfactory, non-enzymatic glucose sensor with high sensitivity and good anti-interference ability.

After the electrochemical measurements the sensor electrode was washed thoroughly using deionized water, then dried in air under ambient conditions. The CV response of this electrode with similar glucose concentrations was carried out after a few days and the result exhibited almost no change in the current response. This proves that the $NiTiO_3$/NiO nanoparticles are a highly stable and reusable glucose biosensor.

Conclusions

In a nutshell, self-assembled $NiTiO_3$/NiO nanocrystals have been synthesized using a simple EISA method using Pluronic F127 and a Ni : Ti 1 : 1 molar ratio in completely non-aqueous ethanolic media. Annealing at 773 K results in a highly crystalline phase of ilmenite $NiTiO_3$ nanoparticles with a rhombohedral (trigonal) structure along with some percentage of a NiO bunsenite phase. The composite $NiTiO_3$/NiO particles with a particle size of 30–35 nm exhibit outstanding electrocatalytic activity towards non-enzymatic glucose detection. A thorough electrochemical investigation of the $NiTiO_3$/NiO nanocomposites using glucose analyte as well as human serum reveals that the material has a very high sensitivity, excellent specificity, good stability, reusability and a very low limit of detection (LOD). Other species like ascorbic acid, dopamine and uric acid show no significant interference in this glucose detection. Hence, the $NiTiO_3$/NiO electrode can be used as a potential candidate for the non-enzymatic detection of glucose.

Acknowledgements

N. Pal and S. Banerjee wish to acknowledge the DAE (Department of Atomic Energy, Government of India) for the financial support. B. Saha thanks CSIR, New Delhi for the senior research fellowship.

References

1 R. P. Andres, J. D. Biefield, J. I. Henderson, D. B. Janes, V. R. Kolagunta, C. P. Kubiak, W. J. Mahoney and R. G. Osifchin, *Science*, 1996, **273**, 1690.
2 A. K. Boal, F. Ilhan, J. E. DeRouchey, T. Thurn-Albrecht, T. P. Russell and V. M. Rotello, *Nature*, 2000, **404**, 746.
3 S. Cho, J.-W. Jang, S. Hwang, J. S. Lee and S. Kim, *Langmuir*, 2012, **28**, 17530.
4 J. Liu, S. Mendoza, E. Roman, M. J. Lynn, R. Xu and A. E. Kaifer, *J. Am. Chem. Soc.*, 1999, **121**, 4304.
5 S. K. Das, M. K. Bhunia and A. Bhaumik, *Dalton Trans.*, 2010, **39**, 4382.
6 C. G. Hardy, L. Ren, S. Mac and C. Tang, *Chem. Commun.*, 2013, **49**, 4373.
7 J. Paget, V. Walpole, M. B. Jorquera, J. B. Edel, M. Urbakh, A. A. Kornyshev and A. Demetriadou, *J. Phys. Chem. C*, 2014, **118**, 23264.
8 P. V. Kamat, *J. Phys. Chem. C*, 2007, **111**, 2834.
9 Z.-Y. Yu, L.-F. Chen and S.-H. Yu, *J. Mater. Chem. A*, 2014, **2**, 10889.
10 P. Poizot, S. Laruelle, S. Grugeon, L. Dupont and J.-M. Tarascon, *Nature*, 2000, **407**, 496.
11 K. Saha, S. S. Agasti, C. Kim, X. Li and V. M. Rotello, *Chem. Rev.*, 2012, **112**, 2739.
12 S. Liu, J. Tian, L. Wang, X. Qin, Y. Zhang, Y. Luo, A. M. Asiri, A. O. Al-Youbi and X. Sun, *Catal. Sci. Technol.*, 2012, **2**, 813.
13 V. Polshettiwar and R. S. Varma, *Green Chem.*, 2010, **12**, 743.
14 Q. Lu, F. Gao and D. Zhao, *Nano Lett.*, 2002, **2**, 725.
15 F. Bosc, A. Ayral, P.-A. Albouy, L. Datas and C. Guizard, *Chem. Mater.*, 2004, **16**, 2208.
16 T. Sakai and P. Alexandridis, *Langmuir*, 2004, **20**, 8426.
17 D. G. Angelescua, M. Vasilescua, M. Anastasescua, R. Baratoiua, D. Donescub and V. S. Teodorescu, *Colloids Surf., A*, 2012, **394**, 57.

18 S. K. Das, M. K. Bhunia, A. K. Sinha and A. Bhaumik, *J. Phys. Chem. C*, 2009, **113**, 8918.
19 R. Bleta, P. Alphonse and L. Lorenzato, *J. Phys. Chem. C*, 2010, **114**, 2039.
20 N. Pal and A. Bhaumik, *Dalton Trans.*, 2012, **41**, 9161.
21 D. Grosso, C. Boissíere, B. Smarsly, T. Brezesinski, N. Pinna, P. A. Albouy, H. Amenitsch, M. Antonietti and C. Sanchez, *Nat. Mater.*, 2004, **3**, 787.
22 J.-Y. Chane-Ching, F. Cobo, D. Aubert, H. G. Harvey, M. Airiau and A. Corma, *Chem. – Eur. J.*, 2005, **11**, 979.
23 A. A. Tahir, M. Mazhar, M. Hamid, K. G. Upul Wijayantha and K. C. Molloy, *Dalton Trans.*, 2009, 3674.
24 F. Tietz, F. J. Dias, B. Dubiel and J. H. Penkalla, *Mater. Sci. Eng., B*, 1999, **68**, 35.
25 S. Anandan, T. Lana-Villarreal and J. J. Wu, *Ind. Eng. Chem. Res.*, 2015, **54**, 2983.
26 E. D. Gaspera, M. Pujatti, M. Guglielmi, M. L. Post and A. Martucci, *Mater. Sci. Eng., B*, 2011, **176**, 716.
27 J. L. Wang, Y. Q. Li, Y. J. Byon, S. G. Mei and G. L. Zhang, *Powder Technol.*, 2013, **235**, 303.
28 S.-H. Chuang, M.-L. Hsieha and D.-Y. Wang, *J. Chin. Chem. Soc.*, 2012, **59**, 628.
29 T. Varga, T. C. Droubay, M. E. Bowden, P. Nachimuthu, V. Shutthanandan, T. B. Bolin, W. A. Shelton and S. A. Chambers, *Thin Solid Films*, 2012, **520**, 5534.
30 J. B. Bellam, M. A. Ruiz-Preciado, M. Edely, J. Szade, A. Jouanneauxa and A. H. Kassiba, *RSC Adv.*, 2015, **5**, 10551.
31 A. Heller and B. Feldman, *Chem. Rev.*, 2008, **108**, 2482.
32 L. C. Clark and C. Lyons, *Ann. N. Y. Acad. Sci.*, 1962, **102**, 29.
33 A. S. Kumar, P. Y. Chen, S. H. Chien and J. M. Zen, *Electroanalysis*, 2005, **17**, 210.
34 A. Umar, R. Ahmad, A. Al-Hajry, S. H. Kim, M. E. Abakera and Y.-B. Hahn, *New J. Chem.*, 2014, **38**, 5873.
35 P. R. Solanki, A. Kaushik, V. V. Agrawal and B. D. Malhotra, *NPG Asia Mater.*, 2011, **3**, 17.
36 M. Fleischmann, K. Korinek and D. Pletcher, *J. Chem. Soc., Perkin Trans. 2*, 1972, 1396.
37 C. Wang, L. Yin, L. Zhang and R. Gao, *J. Phys. Chem. C*, 2010, **114**, 4408.
38 M. U. Anu Prathap, B. Kaur and R. Srivastava, *J. Colloid Interface Sci.*, 2012, **381**, 143.
39 X. Li, A. Hu, J. Jiang, R. Ding, J. Liu and X. Huan, *J. Solid State Chem.*, 2011, **184**, 2738.
40 L. S. Hu, K. F. Huo, R. S. Chen, B. Gao, J. J. Fu and P. K. Chu, *Anal. Chem.*, 2011, **83**, 8138.
41 Z.-D. Gao, Y. Han, Y. Wang, J. Xu and Y.-Y. Song, *Sci. Rep.*, 2013, **3**, 3323.
42 K. Huo, Y. Li, R. Chen, B. Gao, C. Peng, W. Zhang, L. Hu, X. Zhang and P. K. Chu, *ChemPlusChem*, 2015, **3**, 576.
43 S. Moghiminia, H. Farsi and H. Raissi, *Electrochim. Acta*, 2014, **132**, 512.
44 M. A. Kiani, M. Abbasnia Tehrani and H. Sayahi, *Anal. Chim. Acta*, 2014, **839**, 26.
45 Y. Liu, H. Teng, H. Houc and T. You, *Biosens. Bioelectron.*, 2009, **24**, 3329.
46 M. Yousef Elahi, H. Heli, S. Z. Bathaie and M. F. Mousavi, *J. Solid State Electrochem.*, 2007, **11**, 273.
47 X. H. Niu, M. B. Lan, H. L. Zhao and C. Chen, *Anal. Chem.*, 2013, **85**, 3561.